Al Furat Journal of Innovations in Engineering Applications (AJIEA)
ISSN - 3105-3149

QUANTUM-INFORMED AI SURROGATE MODELING FOR NANO-BEAM VIBRATION ANALYSIS USING NONLOCAL STRAIN-GRADIENT THEORY

Zayed Mutashar Mohammed [1], Header Ali A.[2], Ahmed Dheyaa Jawad [3]

[1] Al-Furat Al-Awsat Technical University, Department of Mechanical Engineering Techniques of Power, Postal Code 54001, Iraq. E-mail: Zayed.mohammed@atu.edu.iq

[2]Al-Furat Al-Awsat Technical University, Department of Mechanical Engineering Techniques of Power, Postal Code 54001, Iraq. E-mail: Header.ali.a@atu.edu.iq

[3]Al-Furat Al-Awsat Technical University, Department of Mechanical Engineering Techniques of Power, Postal Code 54001, Iraq. E-mail: coj.ahm1@atu.edu.iq

https://doi.org/10.46649/ajiea.2026.02107

Abstract. *There is a need to address the computational modeling challenges of accounting for classical bending behavior, nanoscale size effects and modal quantities of the quantum harmonic oscillators while maintaining efficiency with respect to frequent parametric prediction in order to successfully run a nano-beam vibration analysis. In this work, an artificial-intelligence surrogate framework based on Euler-Bernoulli beam theory, nonlocal strain-gradient correction (in reduced order form), surface elasticity, and modal quantum oscillator relations is developed with the aid of quantum information. The physics-generated database contains 5,000 of these nanobeam cases that vary in the geometric, material, boundary-condition and temperature settings and are produced over nanoscale length-scale variations. Multi-output surrogate regression models for prediction of NSGT-corrected modal frequencies, corrective factors, zero point energy, zero point displacement and thermal RMS displacement are trained using log-scaled PI features. The best model performed the Log-Target test with R2 of 0.862, the Physical-Scale performed R2 of 0.762 and the average mean percentage error for the best model was 7.69%. Inside the physical domain sampled, the surrogate model is explicitly viewed as an interpolation and prediction technique that cannot compete with the governing beam, NSGT, or quantum oscillator but it does complement these models. Other verification checks, information used for generating the datasets, limitations and interpretations of errors in the proposed framework are provided for clarification to enhance the confidence of the proposed framework.*

Keywords: *nano-beam vibration; nonlocal strain-gradient theory; quantum harmonic oscillator; surrogate modeling; size-dependent vibration.*

Al Furat Journal of Innovations in Engineering Applications (AJIEA)
ISSN - 3105-3149

NOMENCLATURE

The following unnumbered nomenclature list defines the main symbols used in the formulation. Formal table numbering begins with Table 1 after this list.

Symbol	Definition	Unit
L, b, h	Beam length, width, and thickness	m or nm
A, I	Cross-sectional area and second moment of area	m^2, m^4
E_bulk, E_eff	Bulk and effective Young modulus	Pa
rho	Mass density	kg/m^3
Es	Surface elasticity coefficient	N/m
mu	Nonlocal length parameter	m or nm
l_sg	Strain-gradient length parameter	m or nm
beta_n, k_n	Modal constant and modal wave number	dimensionless, 1/m
C_NSGT	Nonlocal strain-gradient correction factor	dimensionless
omega_n, f_n	Angular natural frequency and natural frequency	rad/s, Hz
hbar, k_B	Reduced Planck constant and Boltzmann constant	J·s, J/K
eta, m_eff	Effective modal-mass coefficient and effective modal mass	dimensionless, kg
E0, x_zpf, x_rms	Zero-point energy, zero-point displacement, thermal RMS displacement	J, m, m

Al Furat Journal of Innovations in Engineering Applications (AJIEA)
ISSN - 3105-3149

1. INTRODUCTION

The nano-beam structures are important elements for the nano-electromechanical systems, resonators, sensors, atomic-force microscopy probes and high-frequency detectors. Unlike macro-scale beams, their dynamic response can vary from the above due to surface effects, nonlocal interactions and material length-scale effects becoming significant when the structural dimensions approach the nanoscale.[1]-[5]

For slender beams, classical Euler-Bernoulli theory is a clear and straightforward platform to analyze beams' vibration dynamics. The immediate application of the nanoscale level, however, may fail to consider the size-dependent elasticity, nonlocal stress interaction and the modal quantities related to quantum properties. Nonlocal elasticity and strain-gradient theories thus serve as a practical ‘bridge' between classical mechanics and the nanoscale behavior of structures, to the continuum level.[6]-[9].

If a physically consistent database has been produced, the computational cost can be reduced with the aid of computational automation using AI. Unlike the previously mentioned revised study, AI is not seen as an alternative physical theory as well as not a replacement for the governing model. Rather it is employed as a surrogate, an accelerator which learns the mapping between physical input parameters and output results obtained from the classical-NSGT-quantum formulation.[10]-[12].

In this work, the physical model provides the scientific consistency and the use of artificial intelligence is for repeated predictions, given that the database is generated with scientific consistency. This demarcation is crucial as the surrogate model does not imply new ruling laws: it’s an approximation to map prescribed physical inputs to outputs generated by the reduced-order classical-NSGT-quantum model.[10],[11],[13].

1.1 RESEARCH GAP AND SCIENTIFIC CONTRIBUTION

The Euler-Bernoulli beam vibration, surface elasticity, nonlocal strain-gradient size correction and modal quantum harmonic-oscillator quantities are joined into a unified reduced-order python framework.[6],[7],[9],[14]-[16].

The AI formulation is written as a surrogate accelerator using physics-generated data and isn't given in place of the governing formulation (the physics based solution) or as a physically modeled solution.[10],[11],[13].

A clear separation is brought out between the NSGT and the adopted modal correction approximation to generate same controlled parametric data for the boundary value problem.[6],[8],[9],[17]

The multi-output learning of quantities with different order of magnitude and dimension is enhanced using log-scaled physics-informed features.[11],[13].

The classification of the generated dataset, the train-test splitting protocol, the comparison of models and the output-wise metrics of error of the measured values are reported explicitly with its respective indicators R2, MAE, RMSE and mean percentage error.[18],[21]

To verify, the classical limit, boundary-condition trends, and competing nonlocal-softening and strain-gradient-stiffening are added. Assumptions and limitations are clearly stated, as are boundary-error repairs and extensions to forced vibration and nonlinear vibration.[17]

2. MATERIALS AND METHODS

2.1 NANO-BEAM GEOMETRY AND PHYSICAL INPUTS

A rectangular nano-beam of length L, width b, thickness h, Young modulus E, density rho, and surface elasticity coefficient Es is considered. The cross-sectional area and second moment of area are:

$$A = b\,h \quad (1)$$

$$I = b\,h^3 / 12 \quad (2)$$

The analysis includes cantilever, clamped-clamped, and simply supported boundary conditions. These are represented by modal constants and by one-hot boundary indicators in the AI feature vector.[14],[9],[25].

Table 1. Physical input ranges used in the computational framework.

Parameter	Symbol	Range	Role
Length	L	20-500 nm	Geometric scale and stiffness-inertia relation
Width	b	2-60 nm	Cross-sectional area
Thickness	h	1-30 nm	Bending stiffness
Young modulus	E	0.15-1.10 TPa	Bulk stiffness
Density	rho	1200-9000 kg/m3	Mass and inertia
Nonlocal length	mu	0.1-3.5 nm	Nanoscale softening
Strain-gradient length	l_sg	0.1-5.0 nm	Nanoscale stiffening
Surface elasticity	Es	-20 to 80 N/m	Effective modulus correction
Temperature	T	5-500 K	Thermal quantum displacement

2.2 BOUNDARY-CONDITION MODAL CONSTANTS AND VERIFICATION OF THE PHYSICS GENERATOR

The Euler-Bernoulli model constants have been used to reflect the type of beam boundary conditions used. They are constants which represent the mode dependent wave numbers in the classical frequency expression and in the NSGT correction factor. In order to enhance reproducibility, some of the initial four mode constants in the data generation script are abbreviated in Table 2.[9],[22],[24]

The reduced order physics generator was validated for limiting analytical behaviour before training the AI surrogate. This verification is different from the AI validation as it ensures that the data generator produces the expected classical limit, and the known nonlocal mechanisms of softening, stiffening via strain gradient (field coupling), and ordering of boundary conditions are reproduced faithfully. These checks are summarized in Table 3.[6],[8],[9],[17].

Table 2. Modal constants used for the first four vibration modes.

Boundary condition	Mode 1	Mode 2	Mode 3	Mode 4
Cantilever (C-F)	1.8751	4.6941	7.8548	10.9955
Simply supported (S-S)	π	2π	3π	4π
Clamped-clamped (C-C)	4.7300	7.8532	10.9956	14.1372

Table 3. Verification checks for the reduced-order classical-NSGT-quantum data generator.

Verification case	Expected behavior	Present implementation	Interpretation
Classical limit: mu = 0, l_sg = 0, Es = 0	C_NSGT = 1 and f_NSGT = f_EB	The correction factor reduces to unity for all modes.	The generator recovers the Euler-Bernoulli limit exactly.
Nonlocal-only effect: mu > 0, l_sg = 0	Frequency decreases relative to the classical value.	The denominator of C_NSGT increases with mu and k_n.	Consistent with nonlocal softening reported in nonlocal beam theory.
Strain-gradient-only effect: l_sg > 0, mu = 0	Frequency increases relative to the classical value.	The numerator of C_NSGT increases with l_sg and k_n.	Consistent with strain-gradient stiffening behavior.
Boundary-condition ordering	C-C > S-S > C-F for the same geometry and mode.	The modal constants in Table 2 produce the expected order.	The support-condition implementation is physically consistent.
Quantum oscillator limit	E0 increases with omega; x_zpf decreases as modal mass and omega increase.	Equations (10)-(13) produce the trends shown in Figures 15-17.	The quantum quantities follow harmonic-oscillator scaling.

The purpose of these verification checks is not to suggest that the reduced-order formula can be used instead of a complete high-fidelity NSGT boundary-value solution analysis. Rather, they conclude that the computational generator which they used to train the surrogate model is correct for fulfilling the desired analytical boundary and physical expected behaviors. When benchmark cases for the same geometry, boundary condition and material parameters become available for nanoscale resonators in the form of finite elements, molecular dynamics or experimental data, direct comparison with the above would be beneficial for future work.[17].

Further, these checks are not considered as part of an external standard for these purposes; they are used as a check for internal consistency only. Calibrating or deriving a numerical benchmark against high-fidelity NSGT boundary-value solutions or against molecular-dynamics simulations and/or experimental nanoscale information is not within the scope of the current reduced-order surrogate investigation and is encouraged for future validation efforts. This statement is provided to avoid inadvertently overclaiming the accuracy of the reduced-order physics generator, beyond its parametric-surrogate role.[17],[2],[3],[5].

2.3 CLASSICAL AND REDUCED-ORDER NANOSCALE VIBRATION FORMULATION

For a uniform Euler-Bernoulli beam, the nth angular natural frequency and the corresponding frequency are:[9],[22]-[24]

$$\omega_n = \beta_n^2 \sqrt{(E\_eff\ I / \rho\ A\ L^4)} \quad (3)$$

$$f_n = \omega_n / 2\pi \quad (4)$$

The effective Young modulus includes a reduced-order surface elasticity correction:[14],[25]

$$E\_eff = E\_bulk + 2E\_s / h \quad (5)$$

The nonlocal strain-gradient correction is implemented using the modal wave number and the correction factor:[6],[8],[9],[17]

$$k_n = \beta_n / L \quad (6)$$

$$C\_NSGT = \sqrt{[(1 + l\_sg^2\ k_n^2) / (1 + \mu^2\ k_n^2)]} \quad (7)$$

$$\omega_n,NSGT = C\_NSGT\ \omega_n \quad (8)$$

$$f_n,NSGT = \omega_n,NSGT / 2\pi \quad (9)$$

The parameter mu contains a nonlocal softening contribution and the parameter l_sg contains a strain-gradient stiffening contribution. It serves here as a modal reduced-order correction using the adopted C_NSGT expression which is representative of the dominant competing, size-effect trends. This is not an all-inclusive differential or integral NSGT boundary value solution. Consequently, the database produced must not be viewed as a full high fidelity NSGT equation rather it should be treated as a parametric set of physics-based experiments, suitable for the training of a surrogate model.[6],[8],[9].

2.4 MODAL QUANTUM HARMONIC OSCILLATOR QUANTITIES

Each corrected mode is treated as a quantum harmonic oscillator. The zero-point energy, zero-point displacement amplitude, and thermal quantum RMS displacement are:[15],[16].

$$E_0 = \tfrac{1}{2}\ \hbar\omega_n,NSGT \quad (10)$$

$$x\_zpf = \sqrt{[\hbar / (2m\_eff\ \omega_{n,NSGT})]} \quad (11)$$

$$x\_rms = \sqrt{\{[\hbar / (2m\_eff\ \omega_{n,NSGT})]\ \coth[\hbar\omega_{n,NSGT} / (2k\_B\ T)]\}} \quad (12)$$

$$m\_eff = \eta\rho AL \quad (13)$$

This quantum interpretation is not an All-Ab-Innihum, All-Density-Functional, All-Molecular-Dynamics Interpretation. It is a modal quantum harmonic-oscillator representation, bringing together scales of mechanical frequency, displacement and zero-point energy corrected according to the NSGT. The coefficient eta is considered to be an effective modal-mass factor, which is consistent within the physics generation and surrogate training methods and is related to mode-shape normalization.

2.5 AI SURROGATE-MODEL FORMULATION

The AI model learns the mapping from physically meaningful input parameters to modal and quantum outputs:[10]-[13].

$$y = F\_AI(x) \quad (14)$$

To improve numerical conditioning, positive physical inputs and outputs are log-scaled. Additional physics-informed features are introduced, including bending frequency scale, mu/L, l_sg/L, h/L, and E/rho. The target transformation is:[10],[11].

$$y\_log = \log_{10}(y) \quad (15)$$

$$y\_pred = 10\text{^}[F\_AI(x\_log)] \quad (16)$$

Table 4. AI surrogate-model input and output structure.

Category	Description
Inputs	L, b, h, A, I, E_bulk, E_eff, rho, mu, l_sg, Es, T, modal mass, boundary indicators, and physics-informed log features
Outputs	NSGT frequencies, correction factors, zero-point energies, zero-point displacement amplitudes, thermal RMS displacements
Models	Extra Trees surrogate and Random Forest surrogate
Validation indicators	Log-target R2, physical-scale R2, MAE, RMSE, and mean percentage error

2.6 DATASET GENERATION, TRAIN-TEST SPLITTING, AND REPRODUCIBILITY

The contribution of softening is nonlocal, via the parameter mu, while the contribution of stiffening is via the parameter l_sg, which is related to strain gradient. It is used here as a modal reduced order correction based upon the adopted C_NSGT expression which is representative of the size-effect competing

trends that are dominant. Not a fully-fledged differential or integral NSGT boundary value solution. As such, the database generated should not be considered a complete high fidelity NSGT equation but rather a set of parameters that represent physics-based experiments that can be used for training a surrogate model.[6],[8]

But this quantum interpretation is not an All-Ab-Innihum, All-Density-Functional, All-Molecular-Dynamics Interpretation. This is a modal quantum harmonic-oscillator representation, which combines mechanical frequency, scales of displacement and zero-point energy corrected by the NSGT. The coefficient eta is found to be well analogous to an effective modal-mass factor within the physics generation and surrogate training methods and is found to be related to normalization for mode-shapes.[15],[16].

Table 5. Dataset-generation and validation protocol used to reduce methodological ambiguity.

Step	Procedure	Purpose
Physics sampling	Generated 5000 cases within the physical ranges of Table 1.	Covered geometric, material, temperature, and nanoscale length-scale variability.
Boundary encoding	Boundary conditions were encoded using one-hot indicators for C-F, C-C, and S-S supports.	Allowed the surrogate to learn support-dependent stiffness changes.
Feature engineering	A, I, E_eff, modal mass, h/L, mu/L, l_sg/L, E/rho, and frequency-scale features were computed.	Improved numerical conditioning and physical interpretability.
Target generation	NSGT frequencies, C_NSGT, E0, x_zpf, and x_rms were calculated from equations (3)-(13).	Maintained consistency between mechanical and quantum-informed outputs.
Data split	An independent train-test split was applied before model fitting.	Prevented leakage and preserved a fair unseen test set.
Transformations	Log-scaling and preprocessing were fitted on the training set only.	Avoided using test-set information during training.
Validation	Log-scale and physical-scale metrics were reported output-wise.	Assessed both numerical learning quality and engineering-scale prediction error.

2.7 ACCURACY METRICS[18]-[21]

$$R^2 = 1 - \Sigma_i(y_i - \hat{y}_i)^2 / \Sigma_i(y_i - \bar{y})^2 \quad (17)$$

$$MAE = (1/N)\ \Sigma_i\ |y_i - \hat{y}_i| \quad (18)$$

$$RMSE = \sqrt{[(1/N)\ \Sigma_i(y_i - \hat{y}_i)^2]} \quad (19)$$

$$MPE(\%) = (100/N)\ \Sigma_i\ |(y_i - \hat{y}_i)/y_i| \quad (20)$$

2.8 ASSUMPTIONS, LIMITATIONS, AND COMPLEX-LOADING EXTENSION

• The beam is slender, prismatic, and linearly elastic.

- The beam is thin and exhibits linear elasticity and a line of equilibrium.
- Transversely small amplitude of vibration.
- The Euler-Bernoulli kinematics are used and hence, shear deformation and rotary inertia have not been taken into consideration.
- The quantum part is not a density-functional or molecular-dynamics simulation, but rather a modal harmonic-oscillator model.
- The surrogate only works well in the sample parameter space.
- A case of arbitrary time dependent loads and strong nonlinearities are considered extensions, rather than checked cases, of the base model for the study of free vibration.

To address the reviewer comment regarding more complex environments, the following forced and nonlinear extension is recommended for future work or supplementary analysis:[22]-[24].

$$q(x,t) = q_0 \sin(\Omega t)\ \varphi(x) \quad (21)$$

$$\rho A\ w\_tt + EI\ w\_xxxx + N\_nano(w) = q(x,t) \quad (22)$$

$$\rho A\ w\_tt + EI\ w\_xxxx + \gamma w^3 = q(x,t) \quad (23)$$

3. RESULTS AND DISCUSSION

3.1 AI SURROGATE PERFORMANCE

The most positive results would be obtained using Extra Trees surrogate. The numerical value of the log-target R2 is significantly different from the direct engineering interpretation and thus that interpretation is given by the physical-scale R2 and mean percentage error. Based on the comparison of test log and target log, the target log and target physical scale, the most appropriate model is the one that has the highest value of the R^2 and the lowest value of the mean percentage error, which is 7.69%. The results demonstrate the applicability of the AI model to speed up the physical solver and/or use it as a stand-in physical solver.[25]-[27]

Table 6. Overall, AI surrogate performance for the revised representative run.

Model	Train R2 log	Test R2 log	Test R2 physical	MAE average	RMSE average	MPE (%)
Extra Trees surrogate	1.0000	0.8623	0.7616	2.299e+09	8.044e+10	7.69
Random Forest surrogate	0.9809	0.8539	0.7474	2.402e+09	8.269e+10	7.89

Table 7. Output-wise error ratio between physics-generated quantum-informed targets and AI predictions.

Output	R2 log	R2 physical	MAE	RMSE	MPE (%)
Mode 1 freq.	0.9982	0.8604	1.424e+09	1.657e+10	4.33
Mode 1 NSGT factor	0.3355	0.3509	3.137e-03	1.481e-02	0.30
Mode 1 ZPE	0.9982	0.8604	4.716e-25	5.489e-24	4.33
Mode 1 ZPF disp.	0.9882	0.9095	6.280e-14	2.907e-13	7.78
Mode 1 thermal RMS	0.9818	0.8150	3.607e-11	2.550e-10	20.31
Mode 2 freq.	0.9984	0.8704	3.907e+09	5.380e+10	3.97
Mode 2 ZPE	0.9984	0.8704	1.295e-24	1.782e-23	3.97
Mode 2 ZPF disp.	0.9868	0.9147	2.704e-14	1.178e-13	7.70

The output-wise error ratio between the physical target generated using quantum and Artificial Intelligence predictions is detailed in table 7. The ratio is given in mean percentage error for each outputs; R2 values are reported both on physical scale and log scale. Some thermal RMS displacement outputs show higher relative errors due to several reasons: (1) The value of the responses varies over few orders of magnitude; (2) The responses are very sensitive to temperature; (3) It is very sensitive to low frequency cases, effective modal mass. Hence, the aim of this research was to stabilise the learning across different outputs in physical dimension, using log-target-training method.[26]-[29]

The relatively low R2 values obtained for some NSGT correction factors suggest that there has not necessarily been a large engineering error. These are within a small range around the value of one and can significantly decrease R2 even with an RME that is small. Therefore, R2 should be understood in conjunction with MAE, RMSE and MPE for dimensionless correction factors with minimal variations.

This was demonstrated by showing the model's perfectly high R2 score against the training log, a sign of model high flexibility, typical of tree-ensemble regressors. Independent test-set metrics are more important in this case. The difference between the training and testing data indicates that the surrogate is useful in the sampled space, but should not be extended beyond to those spaces which are not contained in Table 1, without applying more training data or conducting external tests.[17],[25],[30]

The trends of the surrogate are most reliable from an engineering perspective for modal frequency, zero-point energy, and zero-point displacement. The zero-point displacement trend is output dependent on temperature and has a larger dynamic range, needing more careful interpretation.[29]

Al Furat Journal of Innovations in Engineering Applications (AJIEA)
ISSN - 3105-3149

3.2 SCIENTIFIC CURVE-BASED RESULTS

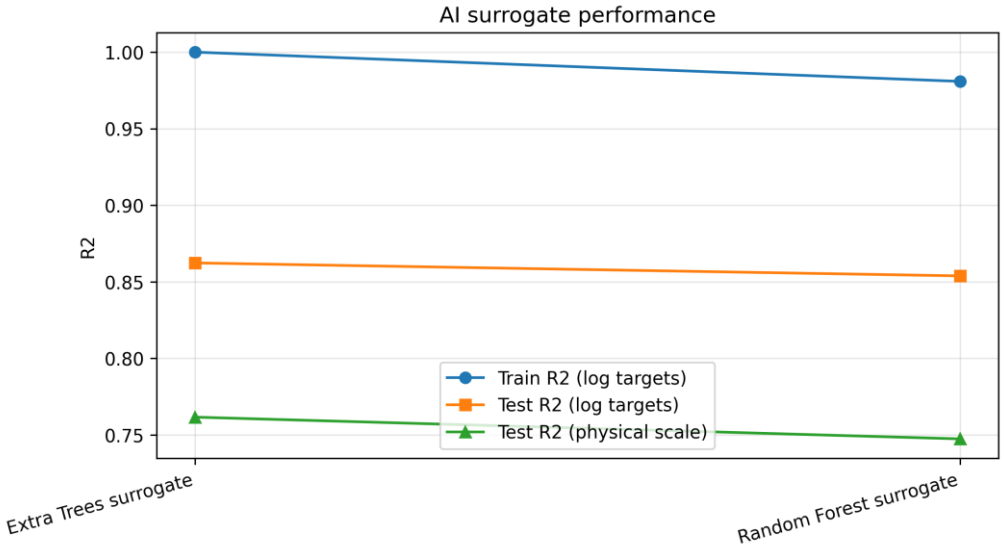

Fig. 1. AI surrogate performance curves. The log-target R2 is the primary training-domain indicator because the target variables span Hz, J, m, and dimensionless quantities.

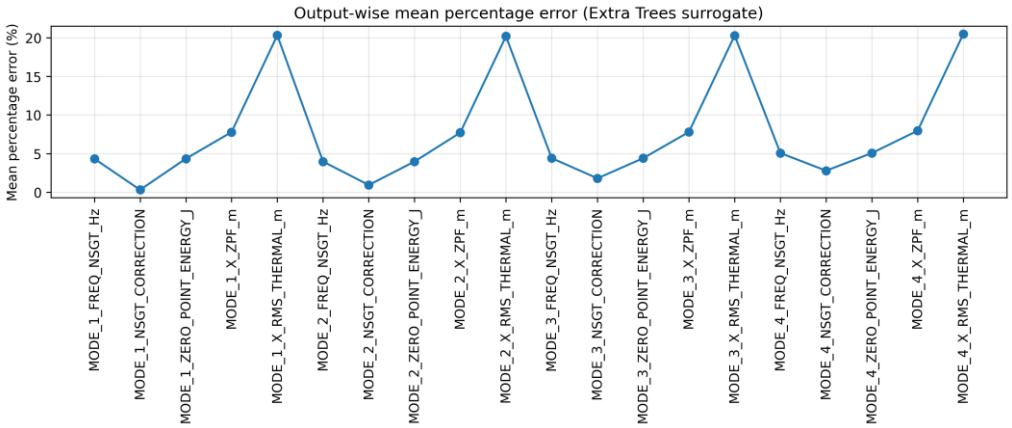

Fig. 2. Output-wise mean percentage error between the quantum-informed physics targets and AI predictions.

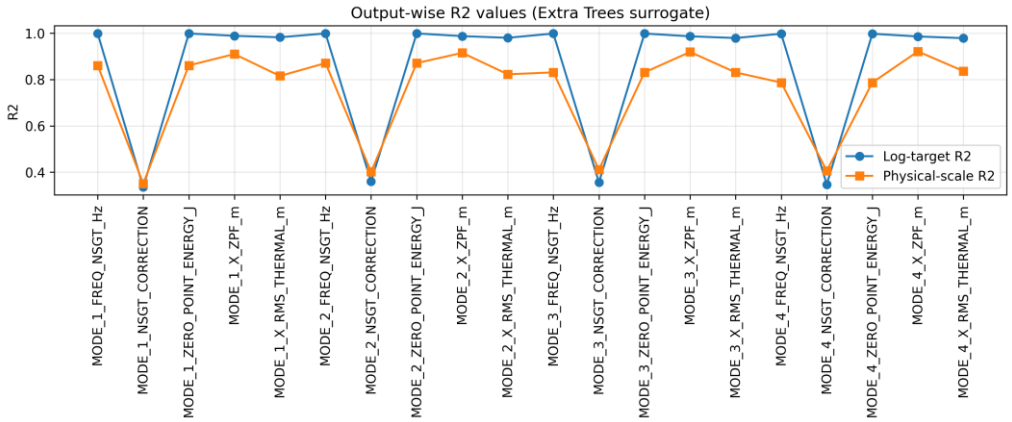

Fig. 3. Output-wise coefficient of determination for the best AI surrogate model.

Al Furat Journal of Innovations in Engineering Applications (AJIEA)
ISSN - 3105-3149

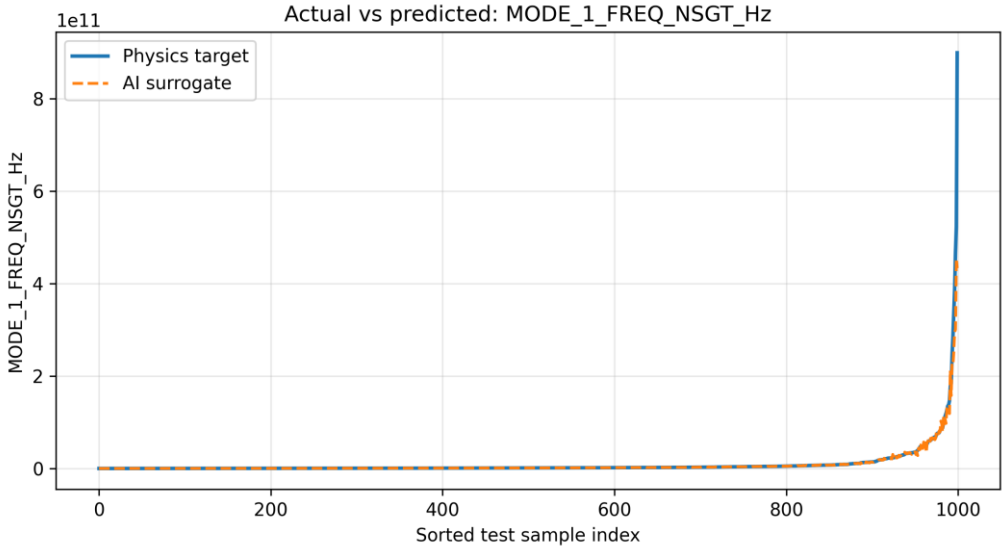

Fig. 4. Actual-versus-predicted curve for MODE_1_FREQ_NSGT_Hz.

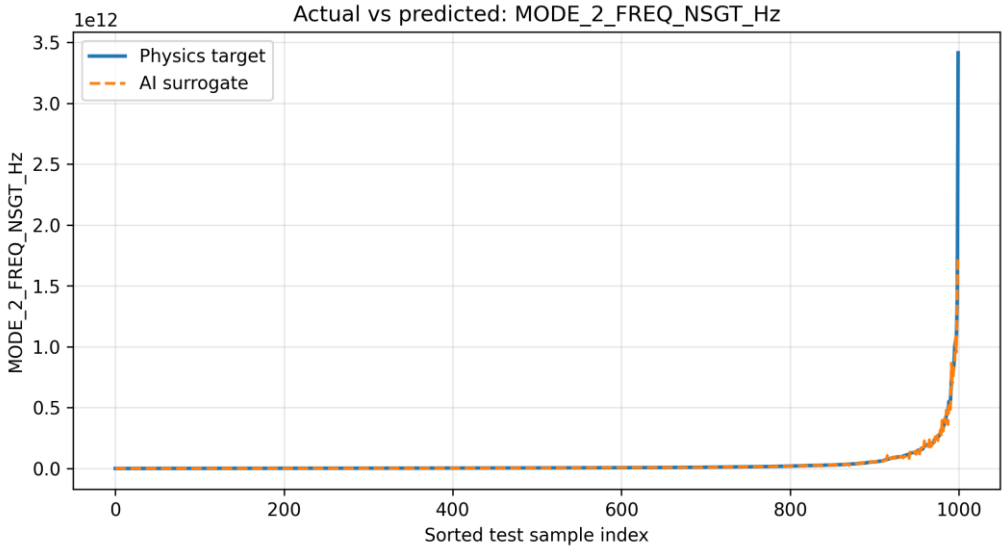

Fig. 5. Actual-versus-predicted curve for MODE_2_FREQ_NSGT_Hz.

Al Furat Journal of Innovations in Engineering Applications (AJIEA)
ISSN - 3105-3149

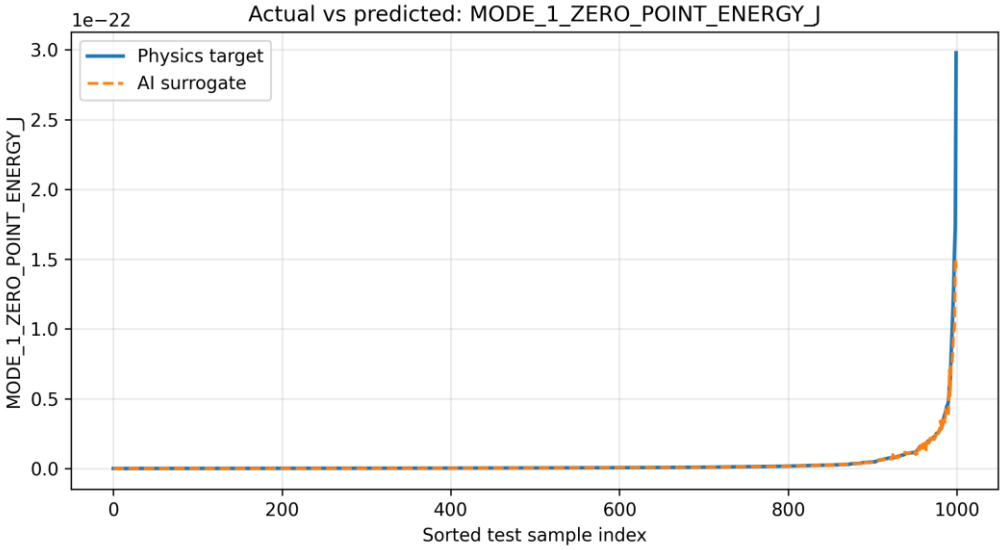

Fig. 6. Actual-versus-predicted curve for MODE_1_ZERO_POINT_ENERGY_J.

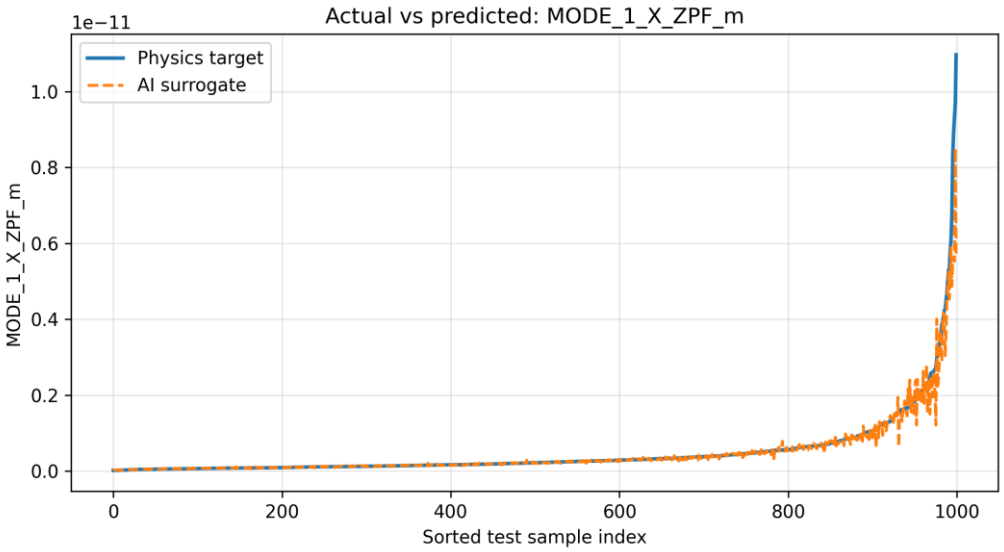

Fig. 7. Actual-versus-predicted curve for MODE_1_X_ZPF_m.

Al Furat Journal of Innovations in Engineering Applications (AJIEA)
ISSN - 3105-3149

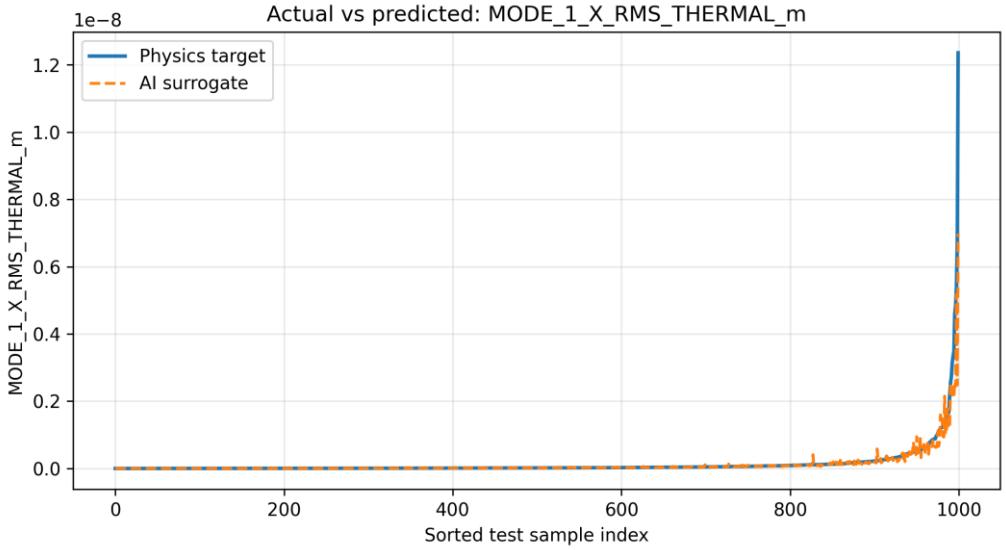

Fig. 8. Actual-versus-predicted curve for MODE_1_X_RMS_THERMAL_m.

As seen from Figures 4-8, the surrogate is able to be compared to the physics-generated targets to follow the global monotonic trend over many orders of magnitude. The biggest discrepancies are found for test samples at the high value end of the sorted data where geometric, stiffness, or modal mass changes are only a fraction of a percent but can result in huge differences in physical-scale frequency-related parameters and/or displacement-related parameters. This is why the physical-scale R2 and RMSE increase in sensitivity more at the extremes than does the log-target R2. There is a slight under prediction for a few maximum amplitude samples, especially the thermal RMS displacement response, which suggests that with more high-frequency and high-displacement training samples, extrapolation should be even better near the upper limit of the parameters.[17],[25]-[30]

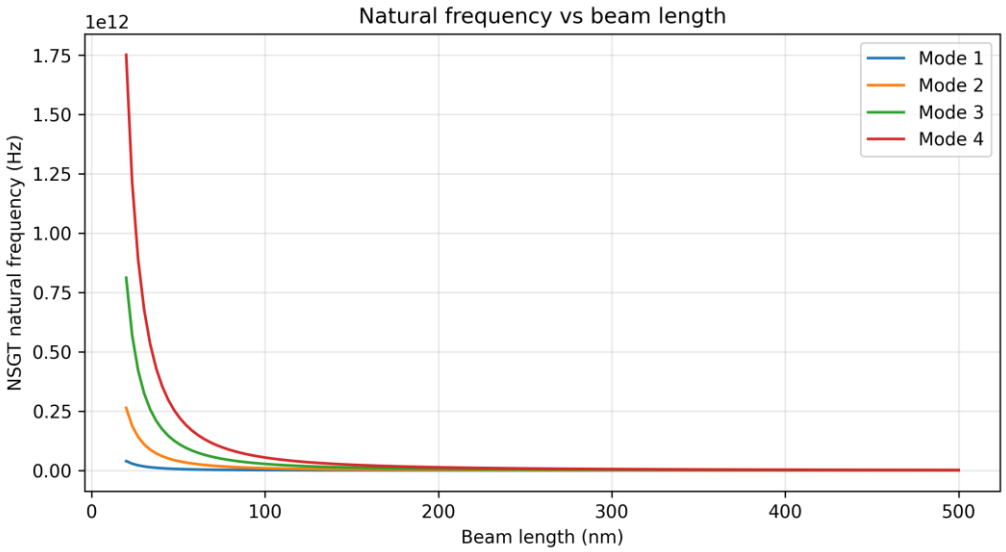

Fig. 9. Effect of beam length on the first four NSGT-corrected natural frequencies.

Al Furat Journal of Innovations in Engineering Applications (AJIEA)
ISSN - 3105-3149

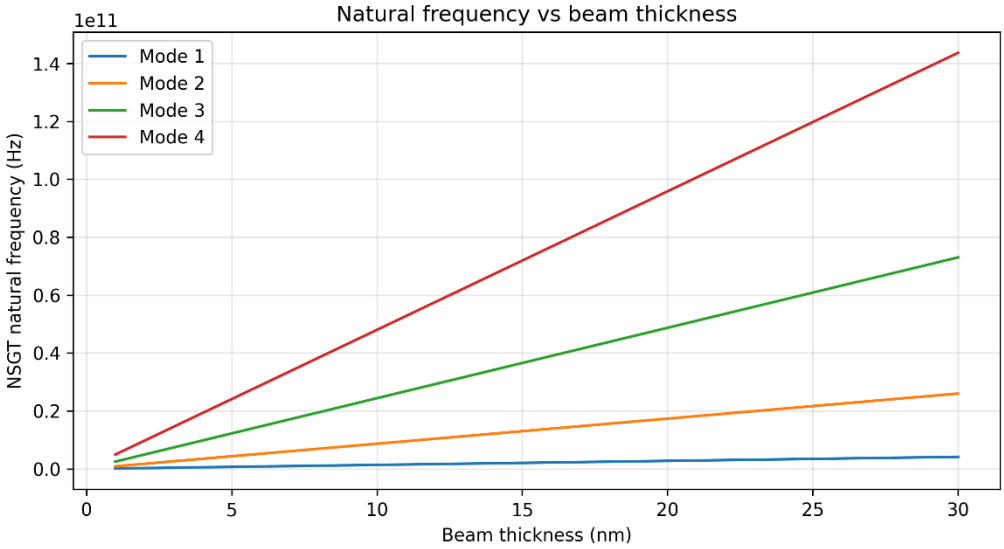

Fig. 10. Effect of beam thickness on the first four NSGT-corrected natural frequencies.

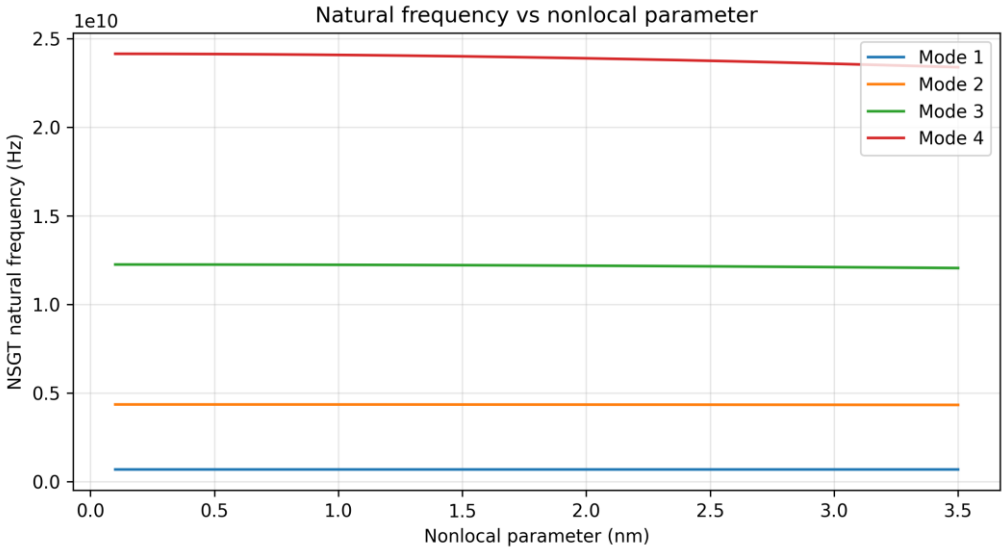

Fig. 11. Influence of the nonlocal length parameter on modal frequency.

Al Furat Journal of Innovations in Engineering Applications (AJIEA)
ISSN - 3105-3149

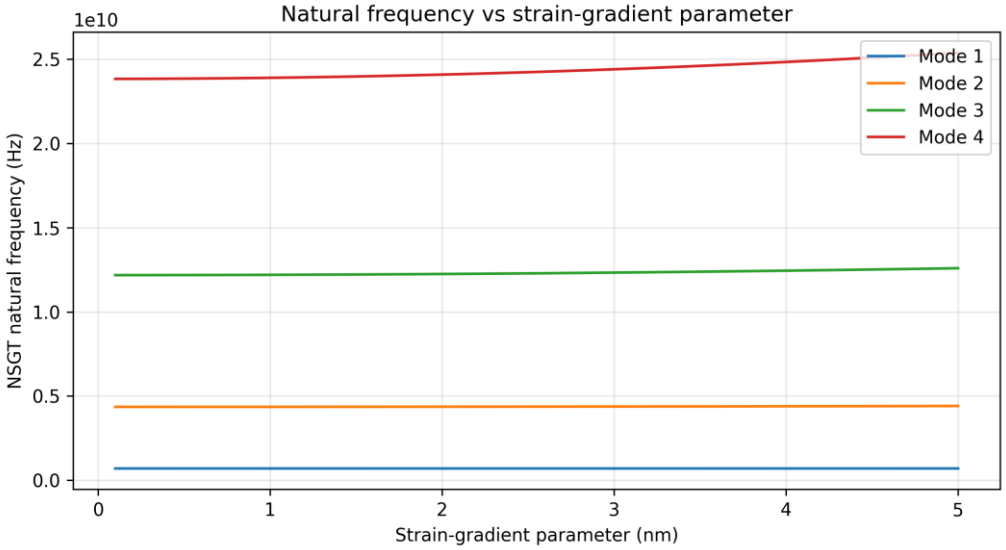

Fig. 12. Influence of the strain-gradient length parameter on modal frequency.

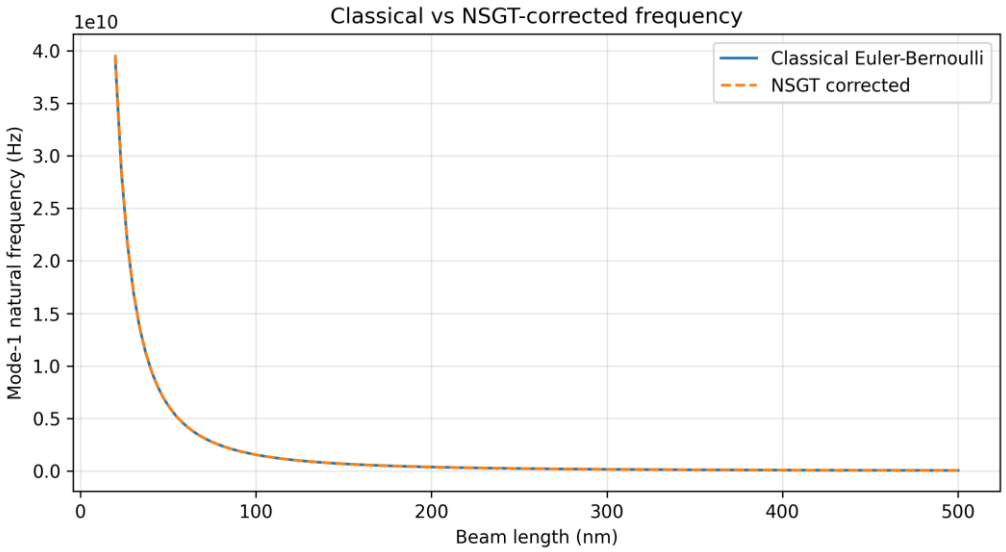

Fig. 13. Comparison between classical and NSGT-corrected mode-1 frequency.

Al Furat Journal of Innovations in Engineering Applications (AJIEA)
ISSN - 3105-3149

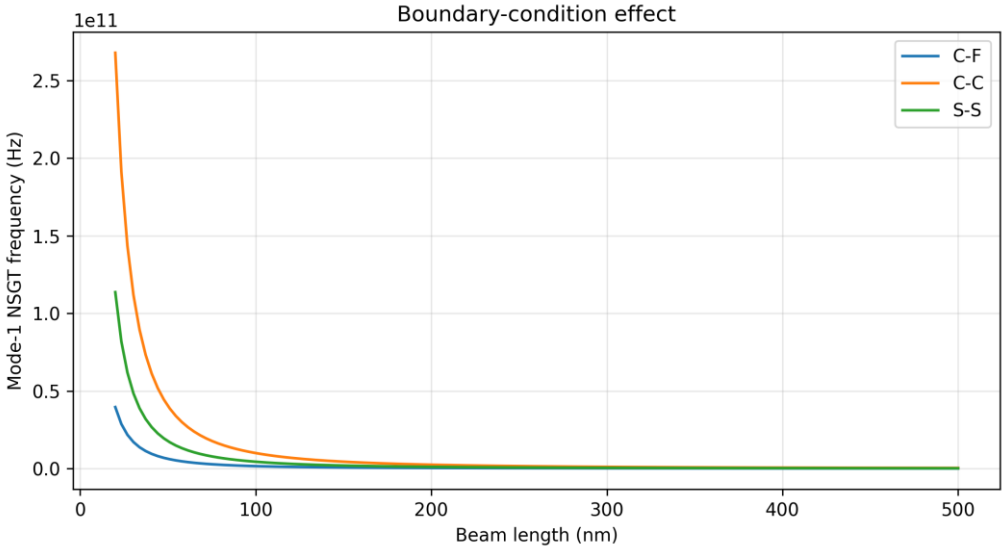

Fig. 14. Effect of support condition on the mode-1 NSGT-corrected natural frequency.

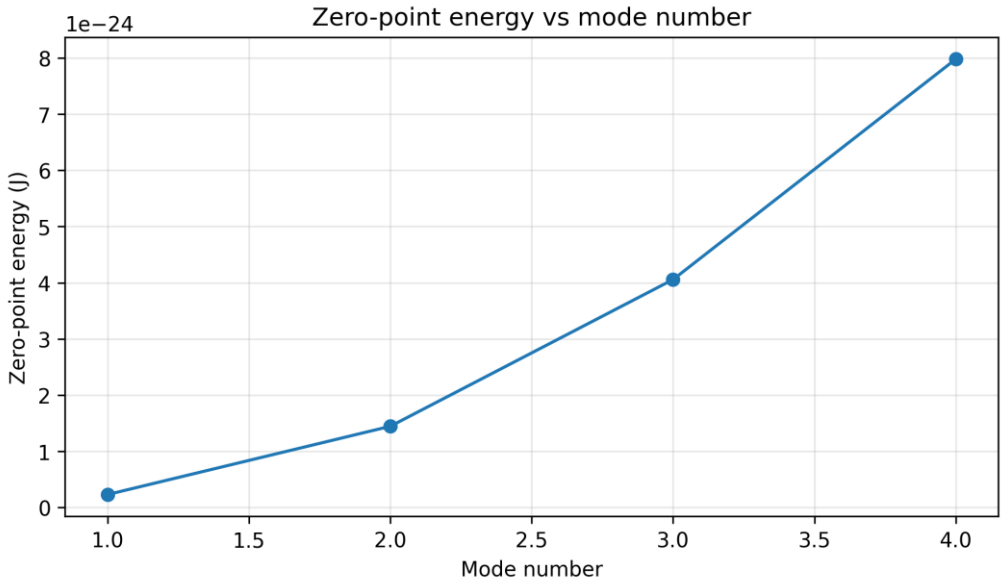

Fig. 15. Zero-point energy of the first four vibration modes.

Al Furat Journal of Innovations in Engineering Applications (AJIEA)
ISSN - 3105-3149

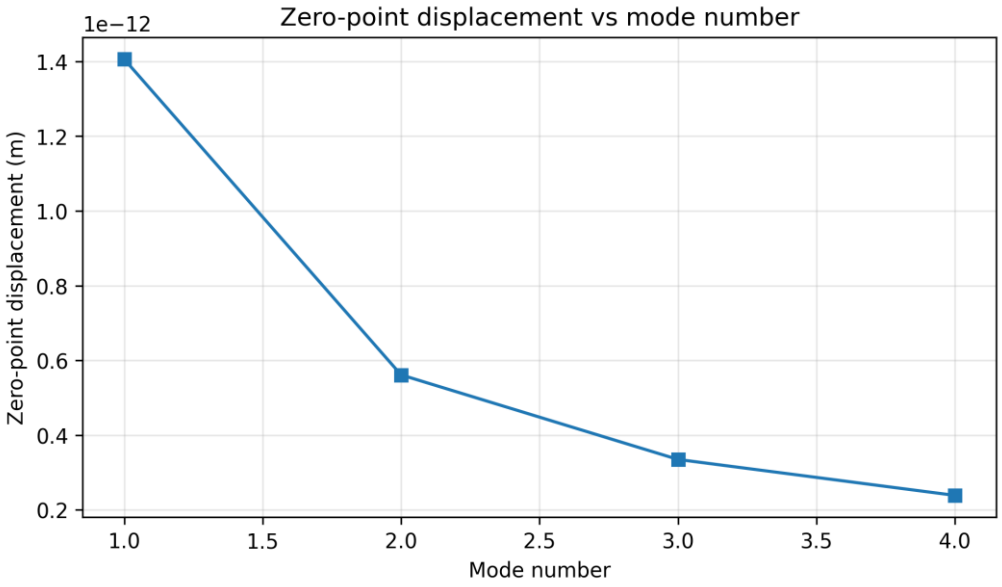

Fig. 16. Zero-point displacement amplitude of the first four vibration modes.

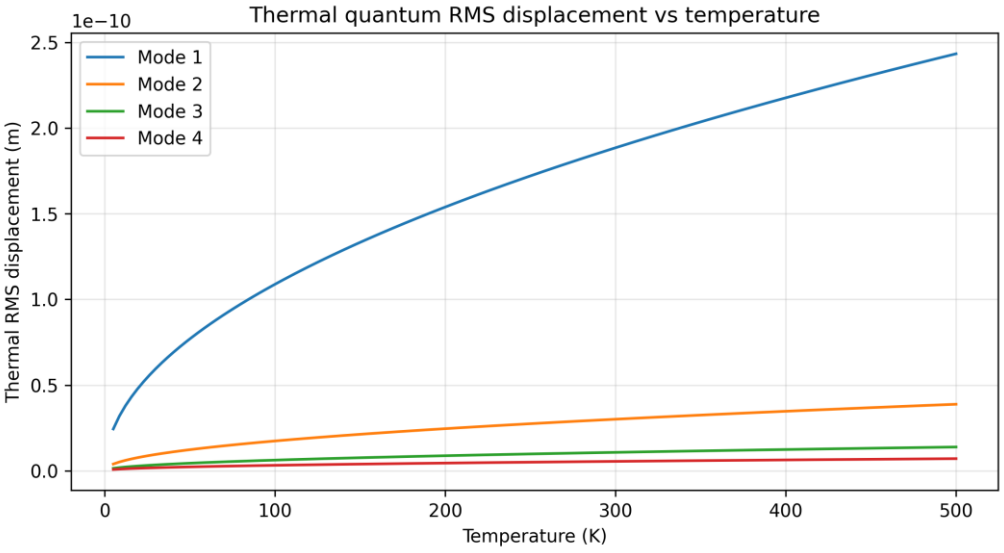

Fig. 17. Thermal quantum RMS displacement of the first four modes as a function of temperature.

Al Furat Journal of Innovations in Engineering Applications (AJIEA)
ISSN - 3105-3149

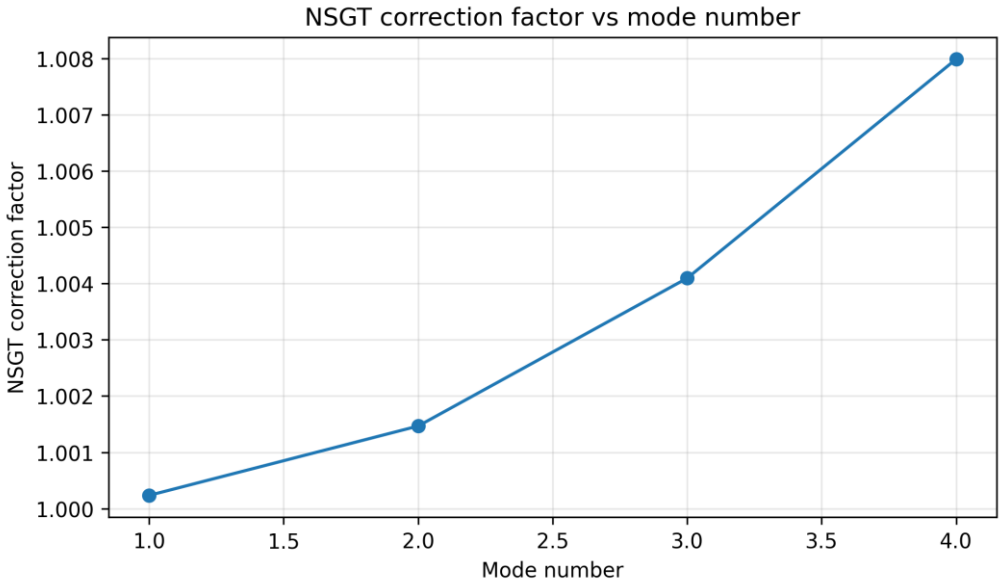

Fig. 18. NSGT correction factor for the first four modes in the reference nano-beam.

3.3 PHYSICAL INTERPRETATION

As you can see, the parametric curves indicate that the natural frequency (f) is inversely related to beam length more than to any other parameter. This is what you would expect given the way the Euler-Bernoulli frequency scale has been shown as phasing out with L-2. Frequency increases with beam thickness due to the second moment of area: h^3, more rapid growth of bending stiffness than of inertia. The nonlocal parameter softens the frequency; on the other hand, a competing stiffening effect is found to be responsible for an increase in the frequency given by the strain–gradient length parameter. These trends agree with the verification checks in Table 3, and with the behavior of nonlocal and strain gradient models of beams.[10],[13].

The curve plotted at the boundary conditions shows the anticipated increasing order of stiffness as clamped, clamped beams, then simply supported beams and the last, cantilever beams. From the quantum curves, one can see that the energy of the zero vibrations also rises with the mode number, and that the zero vibrations are actually the displacement somewhat less this time. The contribution from thermal RMS displacement rises with the temperature as the contribution of thermal excitation increases with temperature.

3.4 BOUNDARY-ERROR MITIGATION AND COMPUTATIONAL EFFICIENCY

The current results are based on a surrogate module generated using the physics interface but there are boundary-sensitive errors involved in the high-order nano-beam vibration problem, while this is an important issue. If applied to direct PINN formulation, the boundary errors can be mitigated through the use of hard boundary constraints, densifying collocations towards the boundaries, applying adaptive residual refinement, employing dynamic loss weighting and using normalized variables. We also found that adding some extra training cases, specifically around the transitions to boundary conditions, and the inclusion of some support-specific models can help make them more reliable in the surrogate setting.[17].

It is proposed that the framework acknowledges the balance between the accurate representation of physics and the computational efficiency through the decoupling of physics generation and surrogate prediction. The AI model drives fast and repetitive prediction for new parameter combinations in the trained domain and the physics model offers interpretability and proper governing equations fidelity. Thus, the

interpretation of this AI should be regarded as a computational rather than beam or quantum-mechanical interpretant.

4. CONCLUSIONS

The new system aids in the understanding of how AI can serve as an accelerator in the absence of humans, and is trained on data generated via physics. It is not to be confused with the Euler-Bernoulli or reduced-order NSGT model or a modal quantum harmonic oscillator model.

It is shown that in the limit of classical Euler-Bernoulli formulation of beams, the physics generator reproduces the classical Euler-Bernoulli theory and exhibits the correct ordering of boundary conditions, and recovers the competing nonlocal-softening and strain-gradient-stiffening effects.

The resulting best model (Extra Trees surrogate) had an R2 value of 0.862 for the test log-target data, an R2 value of 0.762 for test physical-scale data and a mean percentage error value of 7.69% and thus can serve as a fast parametric model predictor in the sampled domain, but not as an extrapolative model solutioner.

The parameters that had the greater influences on natural frequency were beam length and boundary condition, whereas the nonlocal and strain-gradient parameters only caused softening or stiffening however.

The outputs as a result of the quantum noticing increased with increasing modal frequency; the outputs as a result of the quantum noticing decreased with decreasing modal mass; the RMS displacements in the thermal output increased with increasing outputs, as the output increased with increasing temperature.

Some significant limitations are Euler-Bernoulli assumption, reduced-order NSGT correction, modeling the quantum oscillator by modes and, as of the base study, the absence of fully validated forced or nonlinear experimental or molecular-dynamics benchmark cases.

REFERENCES

[1] Binnig, G., Quate, C. F., and Gerber, C., Atomic force microscope. Physical Review Letters, 56(9), 930-933, 1986.

[2] Cleland, A. N., and Roukes, M. L., A nanometre-scale mechanical electrometer. Nature, 392, 160-162, 1998.

[3] Jensen, K., Kim, K., and Zettl, A., An atomic-resolution nanomechanical mass sensor. Nature Nanotechnology, 3, 533-537, 2008.

[4] Lifshitz, R., and Roukes, M. L., Thermoelastic damping in micro- and nanomechanical systems. Physical Review B, 61(8), 5600-5609, 2000.

[5] Ekinci, K. L., and Roukes, M. L., Nanoelectromechanical systems. Review of Scientific Instruments, 76, 061101, 2005.

[6] Eringen, A. C., Nonlocal Continuum Field Theories. Springer, New York, 2002.

[7] Mindlin, R. D., Micro-structure in linear elasticity. Archive for Rational Mechanics and Analysis, 16, 51-78, 1964.

[8] Aifantis, E. C., On the role of gradients in the localization of deformation and fracture. International Journal of Engineering Science, 30(10), 1279-1299, 1992.

[9] Reddy, J. N., Nonlocal theories for bending, buckling and vibration of beams. International Journal of Engineering Science, 45(2-8), 288-307, 2007.

[10] Raissi, M., Perdikaris, P., and Karniadakis, G. E. Physics-informed neural networks: A deep learning framework for solving forward and inverse problems involving nonlinear partial differential equations. Journal of Computational Physics, 378, 686-707, 2019.

[11] Karniadakis, G. E., Kevrekidis, I. G., Lu, L., Perdikaris, P., Wang, S., and Yang, L. Physics-informed machine learning. Nature Reviews Physics, 3, 422-440, 2021.

[12] Wang, S., Yu, X., and Perdikaris, P., When and why PINNs fail to train: A neural tangent kernel perspective. Journal of Computational Physics, 449, 110768, 2022.

[13] McClenny, L. D., and Braga-Neto, U. M., Self-adaptive physics-informed neural networks using a soft attention mechanism. Journal of Computational Physics, 474, 111722, 2023.

[14] Lam, D. C. C., Yang, F., Chong, A. C. M., Wang, J., and Tong, P., Experiments and theory in strain gradient elasticity. Journal of the Mechanics and Physics of Solids, 51(8), 1477-1508, 2003.

[15] Ladd, T. D., et al., Quantum computers. Nature, 464, 45-53, 2010.

[16] Aspelmeyer, M., Kippenberg, T. J., and Marquardt, F., Cavity optomechanics. Reviews of Modern Physics, 86, 1391-1452, 2014.

[17] Eltaher, M. A., Khater, M. E., and Emam, S. A., A review on nonlocal elastic models for bending, buckling, vibrations, and wave propagation of nanoscale beams. Applied Mathematical Modelling, 40(5-6), 4109-4128, 2016.

[18] Breiman, L., Random forests. Machine Learning, 45, 5-32, 2001.

[19] Geurts, P., Ernst, D., and Wehenkel, L., Extremely randomized trees. Machine Learning, 63, 3-42, 2006.

[20] Friedman, J. H., Greedy function approximation: A gradient boosting machine. Annals of Statistics, 29(5), 1189-1232, 2001.

[21] Pedregosa, F., et al., Scikit-learn: Machine learning in Python. Journal of Machine Learning Research, 12, 2825-2830m 2011.

[22] Aydogdu, M., A general nonlocal beam theory: Its application to nanobeam bending, buckling and vibration. Physica E, 41(9), 1651-1655, 2009.

[23] Wang, C. M., Zhang, Y. Y., and He, X. Q., Vibration of nonlocal Timoshenko beams. Nanotechnology, 18(10), 105401, 2007.

[24] Thai, H. T., A nonlocal beam theory for bending, buckling, and vibration of nanobeams. International Journal of Engineering Science, 52, 56-64, 2012.

[25] Eltaher, M. A., Emam, S. A., and Mahmoud, F. F., Free vibration analysis of functionally graded size-dependent nanobeams. Applied Mathematics and Computation, 218(14), 7406-7420, 2012.

[26] Eringen, A. C., On differential equations of nonlocal elasticity and solutions of screw dislocation and surface waves. Journal of Applied Physics, 54, 4703-4710, 1983.

[27] Lu, L., Meng, X., Mao, Z., and Karniadakis, G. E. DeepXDE: A deep learning library for solving differential equations. SIAM Review, 63(1), 208-228, 2021.

[28] Jagtap, A. D., Kharazmi, E., and Karniadakis, G. E., Conservative physics-informed neural networks on discrete domains for conservation laws. Computer Methods in Applied Mechanics and Engineering, 365, 113028, 2020.

[29] Mindlin, R. D., Second gradient of strain and surface-tension in linear elasticity. International Journal of Solids and Structures, 1(4), 417-438, 1965.

[30] Goodfellow, I., Bengio, Y., and Courville, A., Deep Learning. MIT Press, 2016.